

Visualization of Pulpal Structures by SWIR in Endodontic Access Preparation

Journal of Dental Research
2024, Vol. 103(13) 1375–1383
© The Author(s) 2024



Article reuse guidelines:
sagepub.com/journals-permissions
DOI: 10.1177/00220345241262949
journals.sagepub.com/home/jdr

L. Benz^{1*}, K. Heck^{1*} , D. Hevisov³, D. Kugelmann², P.-C. Tseng¹ ,
Z. Sreij¹, F. Litzenburger¹ , J. Waschke², F. Schwendicke¹ , A. Kienle³,
R. Hickel¹, K.-H. Kunzelmann¹, and E. Walter¹ 

Abstract

Endodontic access preparation is one of the initial steps in root canal treatments and can be hindered by the obliteration of pulp canals and formation of tertiary dentin. Until now, methods for direct intraoperative visualization of the 3-dimensional anatomy of teeth have been missing. Here, we evaluate the use of shortwave infrared radiation (SWIR) for navigation during stepwise access preparation. Nine teeth (3 anteriors, 3 premolars, and 3 molars) were explanted *en bloc* with intact periodontium including alveolar bone and mucosa from the upper or lower jaw of human body donors. Analysis was performed at baseline as well as at preparation depths of 5 mm, 7 mm, and 9 mm, respectively. For reflection, SWIR was used at a wavelength of 1,550 nm from the occlusal direction, whereas for transillumination, SWIR was passed through each sample at the marginal gingiva from the buccal as well as oral side at a wavelength of 1,300 nm. Pulpal structures could be identified as darker areas approximately 2 mm before reaching the pulp chamber using SWIR transillumination, although they were indistinguishable under normal circumstances. Furcation areas in molars appeared with higher intensity than areas with canals. The location of pulpal structures was confirmed by superimposition of segmented micro-computed tomography (μ CT) images. By radiomic analysis, significant differences between pulpal and parapulpal areas could be detected in image features. With hierarchical cluster analysis, both segments could be confirmed and associated with specific clusters. The local thickness of μ CTs was calculated and correlated with SWIR transillumination images, by which a linear dependency of thickness and intensity could be demonstrated. Lastly, by *in silico* simulations of light propagation, dentin tubules were shown to be a crucial factor for understanding the visibility of the pulp. In conclusion, SWIR transillumination may allow direct clinical live navigation during endodontic access preparation.

Keywords: optical imaging, root canal therapy, spatial navigation, dental pulp cavity, x-ray microtomography, Monte Carlo method

Introduction

Root canal treatment (RCT) is a common dental procedure in which infected or inflamed pulpal tissue is removed from the root canals of teeth. Worldwide, about 8.2% of teeth undergo RCT, with more than half of the global population older than 18 y of age (55.7%) having had at least one RCT (León-López et al. 2022). Identifying and accessing the root canal system is the first step during the procedure. Factors such as extensive carious defects (Langeland 1987), restorations (Fleig et al. 2017), or advanced patient age (Carvalho and Lussi 2017) can lead to potential obstructions in the root canal system. These make therapy more difficult and contribute to endodontic failures, with missed canals (15.8%) and iatrogenic perforations (11.8%) being common reasons (Yamaguchi et al. 2018). The overall prevalence of perforations in root canal-treated teeth has been described to be approximately 2.3% to 2.7% (Eleftheriadis and Lambrianidis 2005; Tsesis et al. 2010), leading to tooth extractions in 4 out of 5 cases. Thus, preventing perforations is paramount.

Tools such as radiographs can provide indirect guidance to the location of canals. Probes are routinely used for canal exploration, and surgical microscopes with high illumination can improve visibility during the procedure (Patel and Rhodes 2007). A recent study with specialists demonstrated that all canals in obliterated teeth could be negotiated with the use of a surgical

¹Department of Conservative Dentistry and Periodontology, LMU Hospital, LMU, Munich, Germany

²Institute of Anatomy, Faculty of Medicine, LMU Munich, Munich, Germany

³Institut für Lasertechnologien in der Medizin und Meßtechnik an der Universität Ulm, Ulm, Germany

*Authors contributing equally to this article.

A supplemental appendix to this article is available online.

Corresponding Author:

E. Walter, Department of Conservative Dentistry and Periodontology, LMU Hospital, Goethestr. 70, LMU, Munich, 80336, Germany.
Email: Elias.Walter@med.uni-muenchen.de

microscope but required in some cases up to 60 min (Kiefner et al. 2017). Nonetheless, achieving successful negotiation of canals necessitates a considerable level of expertise. Therefore, there is still a need for tools to simplify primary access preparation and directly visualize tooth anatomy in dentin.

In recent years, light-based noninvasive visualization of biological tissues has emerged as a promising advancement in medicine (Thimsen et al. 2017). In particular, shortwave infrared radiation (SWIR) can penetrate deeper into tissues compared with visible light primarily due to reduced scattering effects (Hong et al. 2017). Dentistry has also embraced SWIR illumination. Every dental tissue type such as enamel, dentin, or pulp has a unique optical behavior defined by absorption, scattering, and refraction in a wavelength-dependent manner (Fried et al. 1995). Moreover, light propagation depends on the microstructure of each tissue. Enamel, for example, consists of aligned carbonated apatite crystals with lower scattering and a higher refraction index than dentin (Zoller et al. 2018). Light propagation in dentin, on the other hand, depends highly on dentin tubules, which behave like long cylindrical tubes and direct light into a forward cone (Kienle et al. 2003). In the presence of a caries, light scattering is increased within the lesion, resulting in reduced light transmission and increased reflection. Transillumination techniques capitalize on this phenomenon by introducing light from the marginal periodontium and assessing transmitted light from the occlusal direction (Heck et al. 2023). The area of the lesion appears darker on the occlusal surface. To the contrary, if illuminated and simultaneously evaluated from the occlusal direction, lesions appear brighter due to reflections (Lederer et al. 2019). In addition, SWIR illumination can increase the contrast of pulp canals and growth lines inside the pulp chamber on the pulp chamber floor (Simon et al. 2021)

Given the distinct optical properties and spatial arrangements of dental tissues, we hypothesize here that SWIR imaging can also reveal the underlying internal tooth anatomy before accessing the pulp chamber inside dentin during endodontic access preparation.

Material and Methods

Tooth Selection and Sample Preparation

Intricate transillumination experiments, in which light is introduced through the marginal gingiva, necessitate a clinically authentic model that incorporates the periodontium. Consequently, human *ex vivo* samples were harvested *en bloc* with intact periodontium including alveolar bone as well as mucosa from the upper or lower jaw from 6 human body donors of the body donor program at the anatomy department, LMU Munich. Out of these, 9 teeth (3 anterior teeth, 3 premolars, and 3 molars) were selected. Samples include clinically realistic and relevant features such as pulp obliterations, caries, or restorations.

Body donors gave their written and informed consent for research purposes, and the local ethical committee of LMU Munich confirmed that no further approval was required.

Each sample was fixed in 3.5% formaldehyde and stored wet at 4 °C.

Experimental Procedure

A stepwise preparation was used to observe optical changes on the cavity floor with increasing preparation depth and thus in an approximation to the pulp chamber by different light-based imaging techniques. At baseline (T0) and, using the tooth cusps as reference points, at preparation depths of 5 mm (T1), 7 mm (T2), and 9 mm (T3), white-light pictures, radiographs, SWIR transillumination (SWIRT), and SWIR reflection (SWIRR) images were taken in full view of the access cavity to compare visual differences on the preparation floor (Fig. 1A).

Image Acquisition

Samples were illuminated by SWIRT at the marginal gingiva from both the buccal as well as oral sides at 1,300 nm (Fig. 1A). For SWIRR, samples were illuminated and evaluated from the occlusal direction at 1,500 nm (Fig. 1A). To compare the internal tooth anatomy to the preparation floor, micro-computed tomography (μ CT) images of the samples were acquired at T2 and segmented into 3-dimensional (3D) tooth models. A detailed description for all imaging methods can be found in the appendix.

Monte Carlo Simulation of Light Propagation

Using Monte Carlo simulations, propagation of light can be effectively simulated *in silico*. These simulations allow for the modulation of specific features or structures to validate their impact on the visual representation in *in vitro* experiments, providing a means for mechanistic insights beyond empirical observation. A detailed description of the simulation procedure can be found in the appendix.

Image Processing, Analysis, and Statistics

To objectively analyze contrasts between the pulp chamber and parapulpal areas, each 3D model was manually aligned to the respective SWIR images by their circumference and used for analysis. Descriptive statistics of image gray values were determined for each area to objectively analyze their differences. These are standardized nowadays as first-order radiomic features and can be determined by PyRadiomics (3.1.0) (van Griethuysen et al. 2017). Further descriptions of the statistical analysis can be found in the appendix.

Results

At first, we evaluated the preparation process with SWIRT and SWIRR imaging (Fig. 1A) and compared the results with white-light photographs and μ CT models.

In general, it can be observed that tooth crowns in the SWIRT images are initially evenly illuminated (Figs. 1–3,

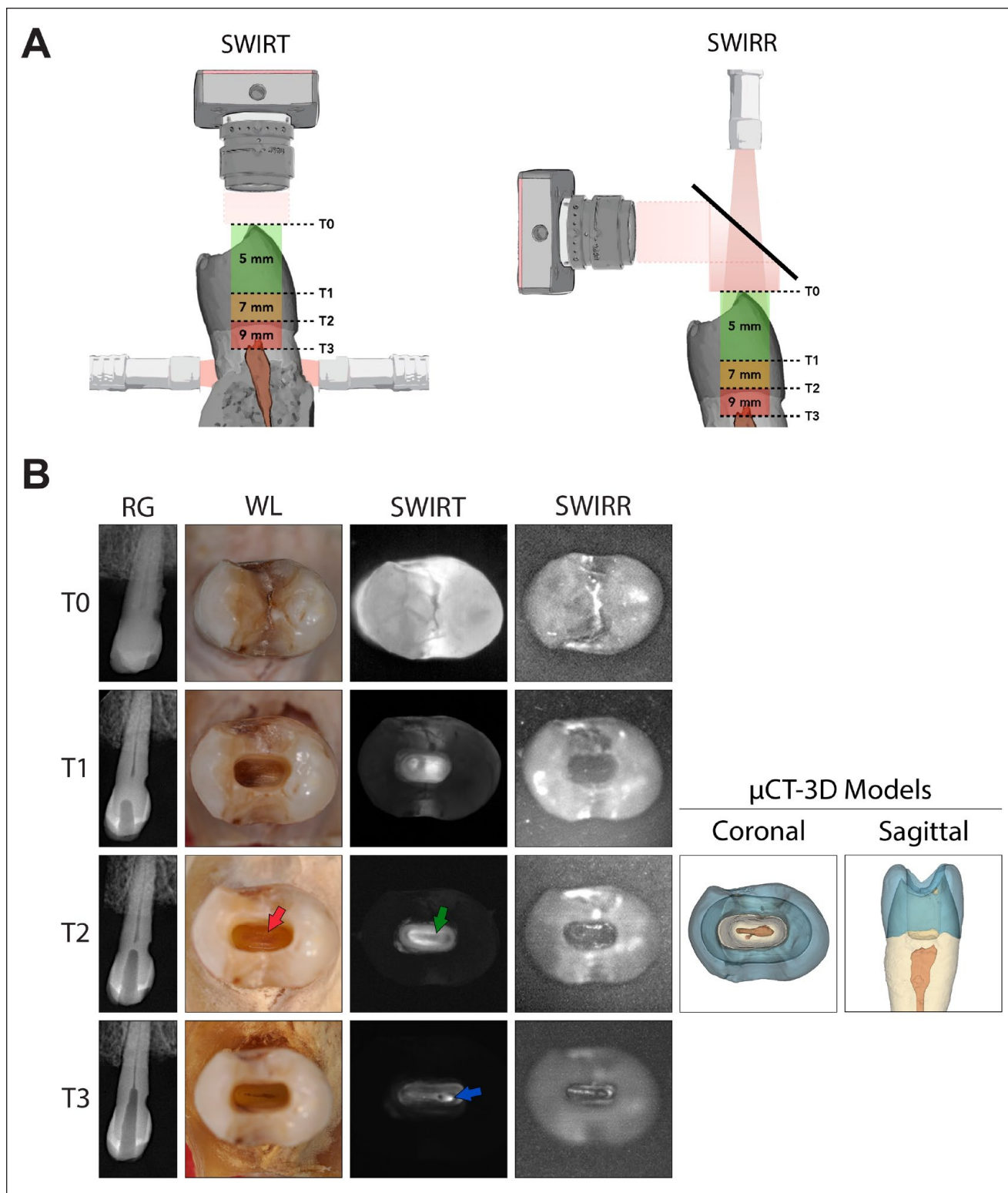


Figure 1. Shortwave-infrared light illumination in premolar teeth. **(A)** Schematic of the experimental setup. **(B)** Representative images of a premolar tooth during stepwise access preparation ($n = 3$). White-light photographs (WVL), radiographs (RG), shortwave infrared transillumination (SWIRT; $\lambda = 1,300 \text{ nm}$), and shortwave-infrared reflection (SWIRR; $\lambda = 1,550 \text{ nm}$) images were taken at each time point (T0 = 0 mm, T1 = 5 mm, T2 = 7 mm, and T3 = 9 mm). Three-dimensional (3D) models of micro-computed tomography (μCT) images at T2 were created to correlate pulpal structures to SWIR images ($n = 3$). The formation of irregular dentin is shown at T2 centrally on the cavity floor in WL (red arrow). Dark areas in the SWIRT image at T2 are correlated with structures of the pulp chamber (green arrow). Upon accessing the pulp at T3, bright spots appear at canal areas where the light source was attached on the outside (blue arrow).

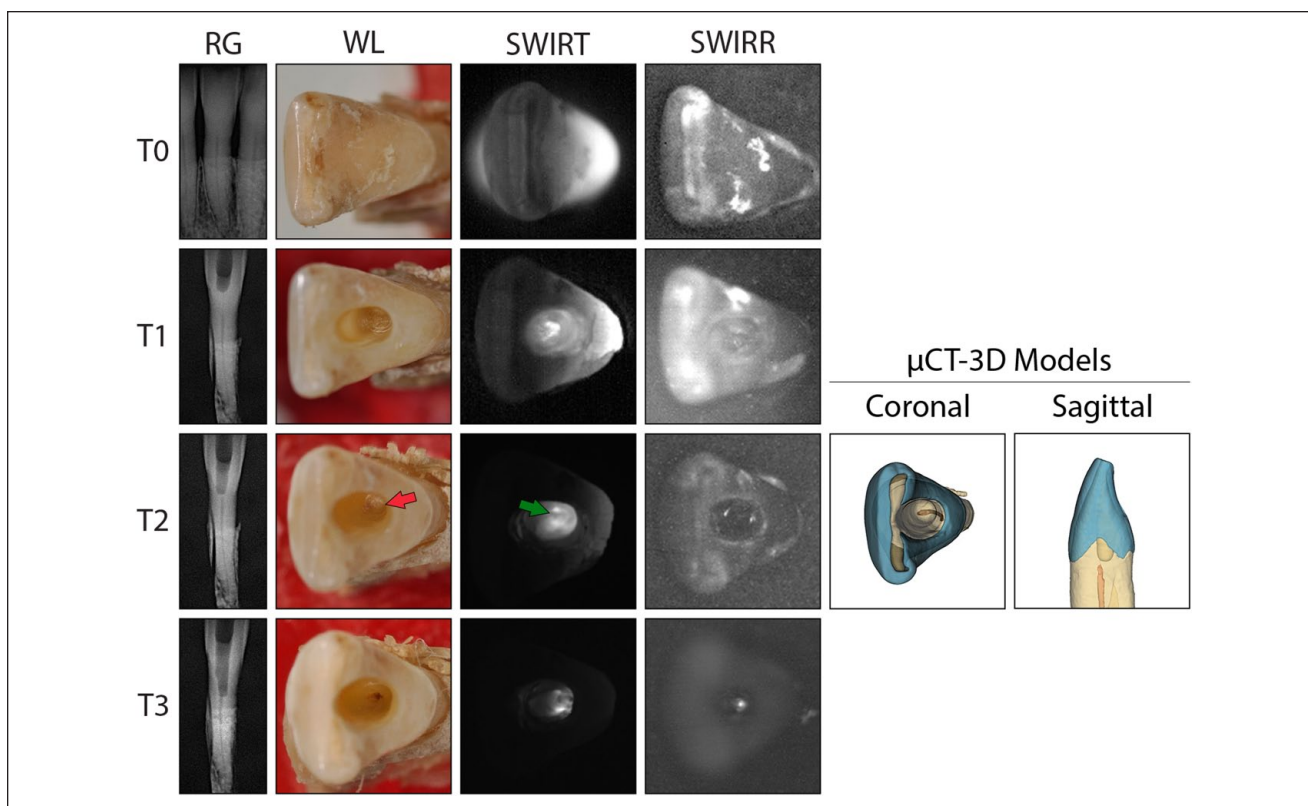


Figure 2. Shortwave infrared light illumination in the anterior teeth. Representative images of an anterior tooth during stepwise access preparation ($n = 3$). White-light photographs (WL), radiographs (RG), shortwave infrared transillumination (SWIRT; $\lambda = 1,300$ nm), and shortwave infrared reflection (SWIRR; $\lambda = 1,550$ nm) images were taken at each time point (T0 = 0 mm, T1 = 5 mm, T2 = 7 mm, and T3 = 9 mm). Three-dimensional (3D) models of micro-computed tomography (μ CT) images at T2 were created to correlate pulpal structures to SWIR images ($n = 3$). The formation of irregular dentin is shown at T2 centrally on the cavity floor in WL (red arrow). Dark areas in the SWIRT image at T2 are correlated with structures of the pulp chamber (green arrow).

SWIRT T0) but appear increasingly darker compared with the preparation cavity, which consecutively appears brighter with increasing preparation depth (Figs. 1–3, SWIRT T1–T3).

In anterior and premolar teeth, the preparation floor has as a homogeneous brown-yellowish surface in white-light images (Figs. 1B and 2; T1 and T2). In some cases, in up to 2 mm distance to the pulp chamber, slightly darker areas can be identified centrally, which indicate irregular dentin (Fig. 1B and 2; T2, red arrows). In SWIRT, a contrast can be identified on the cavity floor (Fig. 1B and 2; T2). Centrally, a darker area is visible and surrounded by a brighter halo in anterior as well as premolar teeth (Fig. 1B and 2; T2, green arrows). This dark area was correlated in 3D segmented μ CT images with the pulp chamber, whereas the halo correlated with parapulpal areas. Similar contrasts were indistinguishable in white-light photographs or SWIRR images (Fig. 4A). Most importantly, the pulp chamber was not accessed.

In an open pulp chamber, these characteristics appear different. Bright spots are visible inside the pulp chamber, approximately at canal areas where the light source was attached on the outside (Figs. 1B and 2; T3, blue arrow).

In molars, white-light images also show the preparation floor approximately 2 mm above the pulp chamber as a

homogeneous brownish surface with some slightly darker areas (Fig. 3; T1, red arrow). In SWIRT images, contrasts can again be identified on the preparation floor, which are indistinguishable in WL or SWIRR (Fig. 4A). Three dark areas can be identified separated by a brighter center. Similarly to observations in anterior and premolar teeth, peripheral areas appear slightly brighter. Correlated with 3D μ CT models, dark areas correspond to locations of canal orifices, while the centrally bright separation is correlated to the furcation of multirooted teeth. Parapulpal areas again presented as a halo.

In an area in which the pulp chamber has been opened, canal areas appear bright in SWIRT images, whereas their appearance is darker in SWIRR images (Fig. 3; T2, blue arrow). However, the cavity floor did not show consistent observations in SWIRR images for all tooth types.

To confirm these observational results, they were objectively analyzed by their gray value features. The μ CT 3D models were used to determine the location of the pulp chamber. They were aligned and superimposed according to the SWIRT images and segmented into pulpal (yellow) and parapulpal (green) areas (Fig. 4B). In first-order features mean and median intensity, variance as well as entropy and energy of the pulp areas were significantly lower than those of the

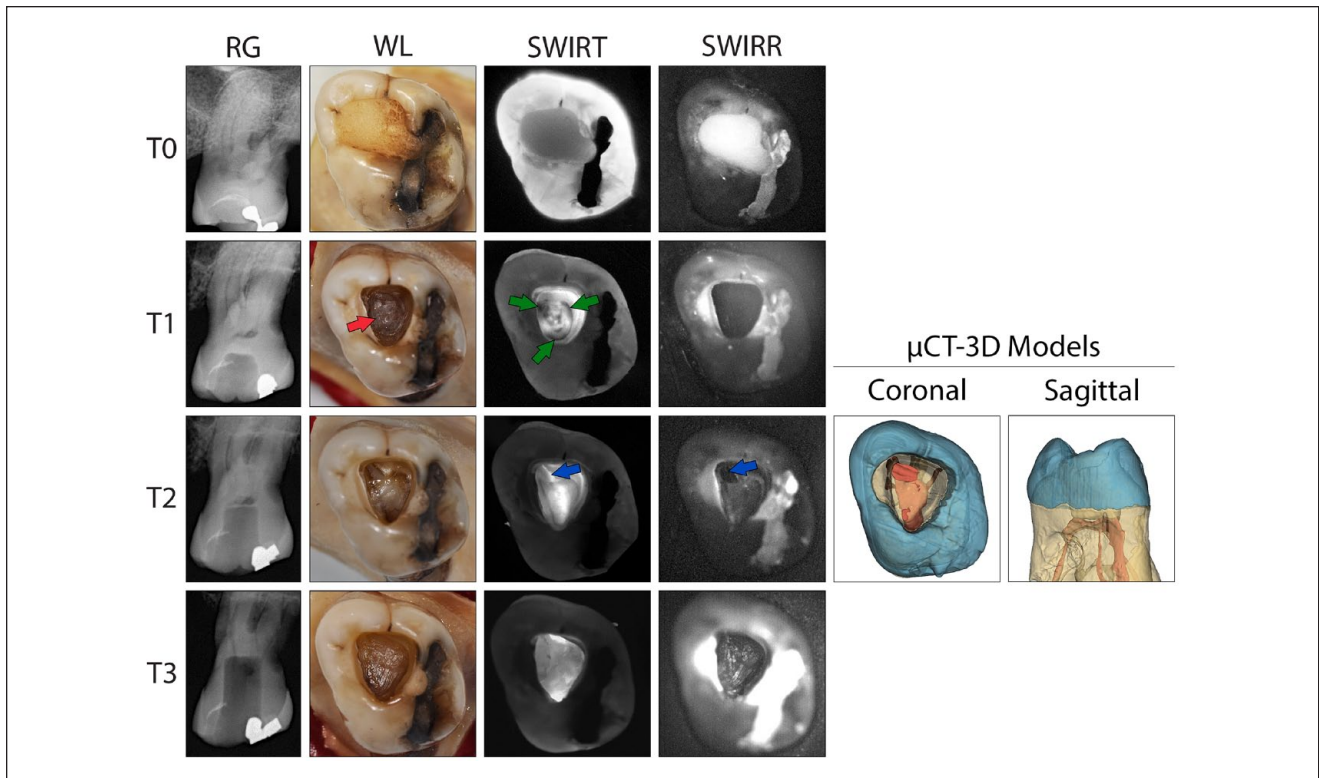


Figure 3. Shortwave infrared light illumination in molar teeth. Representative images of a molar tooth during stepwise access preparation ($n = 3$). White-light photographs (WL), radiographs (RG), shortwave infrared transillumination (SWIRT; $\lambda = 1,300$ nm), and shortwave infrared reflection (SWIRR; $\lambda = 1,550$ nm) images were taken at each time point (T0 = 0 mm, T1 = 5 mm, T2 = 7 mm, and T3 = 9 mm). Three-dimensional (3D) models of micro-computed tomography (μ CT) images at T2 were created to correlate pulpal structures to SWIR images ($n = 3$). The formation of irregular dentin is shown at T1 centrally on the cavity floor in WL (red arrow). Dark areas in the SWIRT image at T1 are located at canal orifices (green arrows). Upon accessing the pulp at T2, bright spots appear at canal areas; in SWIR images, these areas appear dark (blue arrows).

parapulpal areas, although they presented with a higher uniformity (Fig. 4C).

All first-order features including statistically nonsignificant features were included in a hierarchical cluster analysis by which specific data and their similarities can be grouped unsupervised to generate specific data patterns. These similarities are arranged in a dendrogram with hierarchical orders (Fig. 4D). In the higher order, 3 distinct groups can be identified for both features (left, middle right) and samples (top, middle, bottom) indicated by a line separation. Almost all pulpal segments are characterized by low values in the left feature group from energy to range and high values in the right group with skewness, kurtosis, and uniformity. All parapulpal areas on the other hand show high values in the left and middle feature group, whereas the right group consists of low values. Parapulpal areas of molars are characterized by a separate subcluster with even higher values in the left feature group.

Next, we investigated the mechanism or factors by which pulpal structures appear darker. The visual representation of these structures may be influenced by the remaining dentin thickness in between preparation and the pulp chamber. Therefore, the Euclidean distance in each area of the tooth was determined in μ CTs and plotted per pixel against the intensity in SWIRT images. A clear increase in intensity with increasing

thickness was recorded in premolars and anterior teeth (Fig. 5A). In molars, due to the homogeneous thickness of the chamber roof but higher intensity in areas with underlying furcation, this behavior is not clearly given. In marginal areas of the cavity, it can nevertheless be observed (Fig. 5B). Both segments were confirmed unsupervised by k-mean clustering (Fig. 5A and B; lower right) and compared with manual segmentations of μ CTs. The similarity between both can be expressed by Fowlkes-Mallow scores. With a mean score of 0.65 ± 0.073 , the unsupervised clustering is in high agreement with the ground truth. The linear regression analysis of centroids shows a high Pearson coefficient (0.76) for all teeth and thus a strong linear dependence of intensity and remaining dentin thickness of the pulp chamber roof (Fig. 5C).

Light propagation in dentin is highly dependent on dentin tubules. Therefore, Monte Carlo simulations were performed on premolars to investigate the influence of dentin tubules on the visual representation of the pulp (Fig. 5D). In simulations lacking dentin tubules, the cavity floor appears homogenous without any discernible structures. The overall light propagation is hindered, the crown appears dark, and only areas on the left and right side close to light entry on the preparation cavity floor appear with slightly higher intensity. Upon adding dentin tubules radially from the center of the pulp, the crown appears

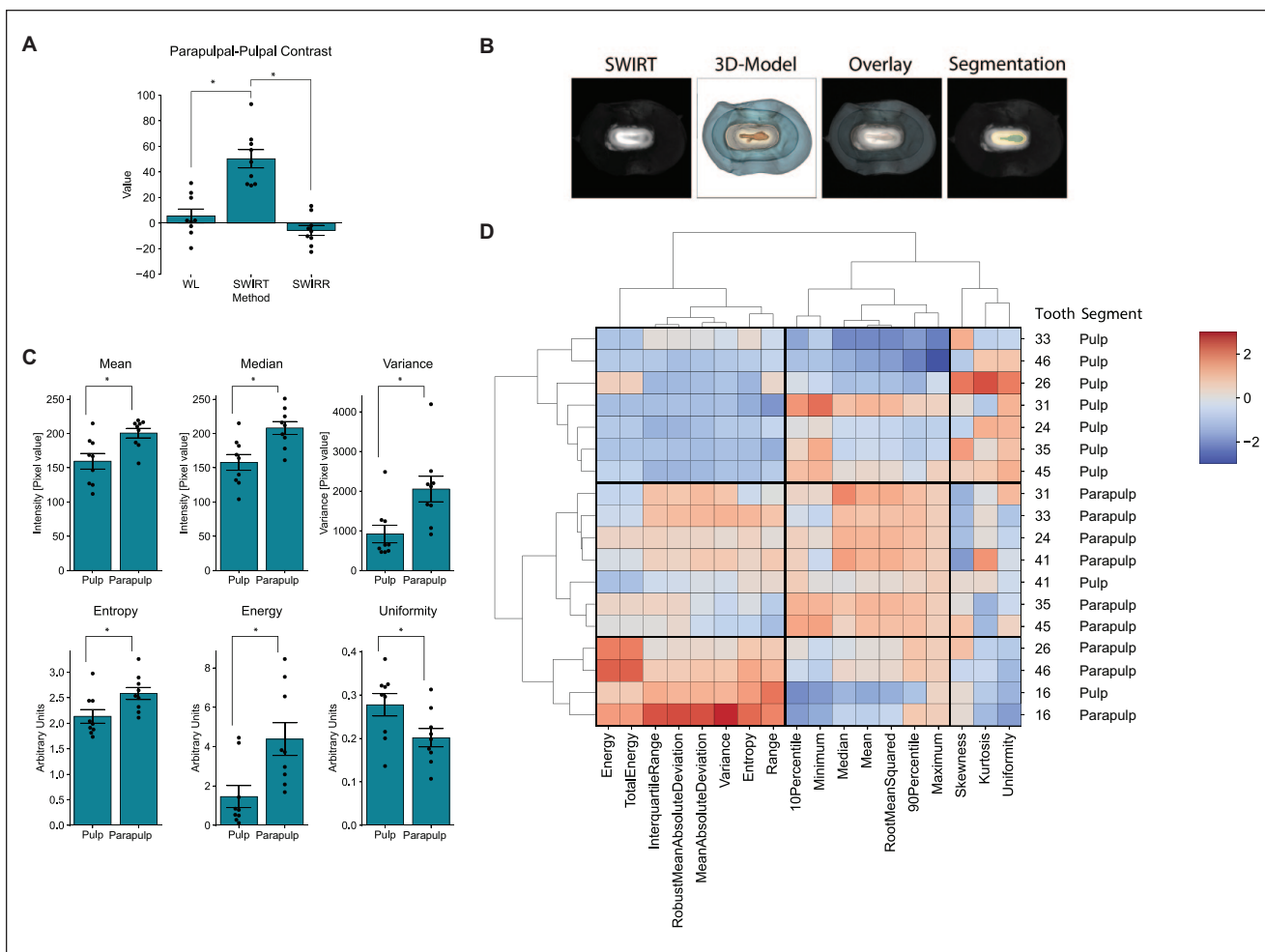


Figure 4. Objective analysis of pulpal and parapulpal areas in SWIRT images. **(A)** Comparison of pulpal and parapulpal contrasts in different image acquisition methods at T2 ($n = 9$, analysis of variance, $*P \leq 0.05$) **(B)** Shortwave infrared transillumination (SWIRT) images and three-dimensional (3D) models of micro-computed tomography (μ CT) at T2 were overlaid and segmented into pulpal and parapulpal structures. **(C)** Radiomic feature analysis and comparison of both segments ($n = 9$, t test, $*P \leq 0.05$). **(D)** Heat map for first-order radiomic features of hierarchical cluster analysis. Lines separate the 3 main clusters, which can be identified for features as well as samples.

brighter. The location of the pulp becomes visible centrally and is surrounded by halo with higher intensity. Both the *ex vivo* SWIRT images as well as the simulation are darker in areas of the pulp chamber, but in the latter, the area is smaller in size and less pronounced.

Discussion

Our study shows for the first time that by SWIRT imaging, the underlying pulpal structures in dentin can be visualized before reaching the pulp chamber. Darker areas in SWIRT images could be correlated to the underlying pulp chamber and differentiated to parapulpal areas. Key questions arise from our results. At what depths is what structure visible by which mechanism?

In our standardized explorative procedure, preparations were made in 2-mm increments, resulting in varying distances to the pulp chamber. The maximum distance in which areas

could be correlated with the pulp chamber was slightly greater than 2 mm. However, further investigations are needed to determine if greater distances exhibit specific optical features during access preparation associated with pulpal structures.

Furthermore, the pulp chamber consists of many parts: pulp horns, chamber, chamber floor, canal orifices, or finally also each canal. Every premolar and anterior tooth in our data set consisted of teeth with one root canal. While teeth with single canals present challenges in separating the pulp chamber into distinct anatomical structures, molars offer clearer distinctions. There, darker areas could be correlated to areas with underlying pulp horns and/or canal orifices, whereas areas with underlying furcation appeared brighter.

Mechanistically, we hypothesized therefore that remaining dentin thickness plays a role in visual representation. With a reduction in dentin thickness, less light might be scattered into the pulp chamber roof, leading to darker areas. Overall, a positive correlation of thickness and intensity could be

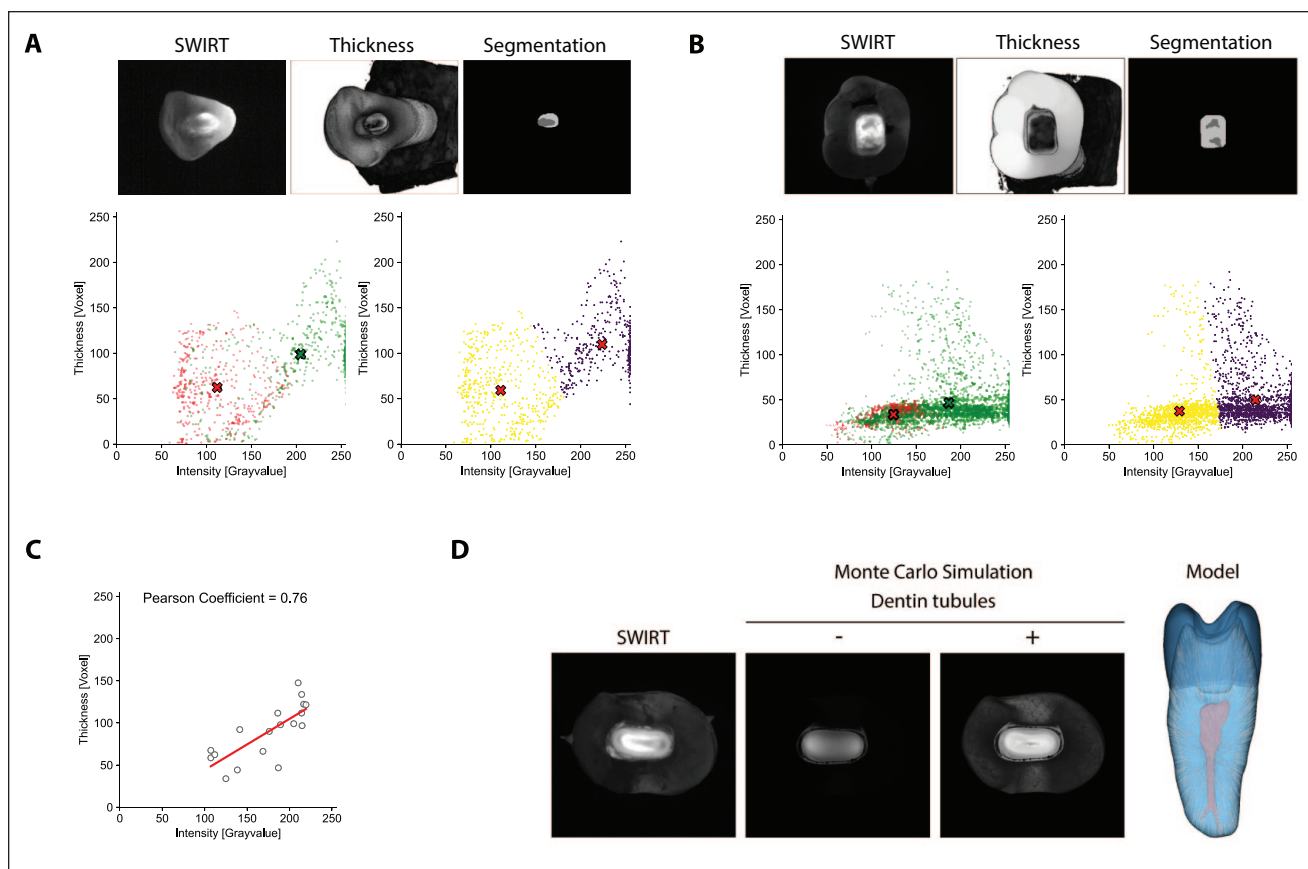


Figure 5. Influence of dentin thickness and tubules on optical projection of the pulp. Shortwave infrared transillumination (SWIRT) images were overlaid with local thickness models based on μ CTs at T2 and compared with segmented pulpal and parapulpal structures. For every pixel in each segment (green = parapulp, red = pulp), both thickness and gray value were determined and plotted (cross = cluster centroid). K-mean cluster analysis confirms both cluster groups. Representative correlation analysis between thickness and gray value of (A) anterior and premolar ($n = 6$) as well as (B) molar teeth ($n = 3$). (C) Linear regression analysis of all centroids ($n = 9$, Pearson coefficient = 0.76). (D) Representative Monte Carlo simulation of light propagation in premolars with and without dentine tubules ($n = 3$).

demonstrated. Nevertheless, dentin thickness above the pulp chamber at furcation areas in molars remained stable while brightness was increased, indicating that dentin thickness is not the only or main contributing factor for the visual projection.

Moreover, light propagation depends on the microstructure of each tissue. Light in dentin is propagated into a forward cone due to dentin tubules (Kienle et al. 2003). In addition, dentin tubules are arranged in a perpendicular direction to the pulp chamber with a bigger size and higher number centrally (Jud et al. 2016). Because of this perpendicular direction, light propagation seems to be directional (Kienle et al. 2006). These optical properties have mostly been investigated in sectioned and barely on complete teeth. The specific impact in areas directly above the dental pulp remains therefore understudied, but they could be the reason for the observed phenomenon by directing light outward away from the pulp chamber.

With the *in silico* simulation, we can indeed demonstrate that dentin tubules are an important factor for understanding the visual projection of the pulp chamber in dentin. But it must be noted that the simulation is based on a simplified version of

dentin tubules and the arrangement as well as density is generated based on other studies (Zoller et al. 2018). It could deviate from the ground truth. In addition, teeth used in this study exhibited secondary dentin formation due to age as well as tertiary dentin due to caries lesions or abrasion. While secondary dentin has a similar histological structure and reactive dentin is practically indistinguishable from primary dentin, reparative dentin comprises a dystrophic, atubular matrix (Smith et al. 1995; Tjäderhane et al. 2009). Therefore, light transmission in these areas could be affected (Berghammer et al. 2022), which is most likely due to changes in tubular structure as well as mineralization. However, their specific optical properties have not yet been investigated. While they can be located in μ CT images (Nudel et al. 2020), each type with its associated microstructure is hard to differentiate. Consequently, neither was included in the simulation. It does therefore not completely fit the associated SWIRT image but proves that even in a simplified version, the pulpal structure is projected into dentin as a darker area. Furthermore, SWIRT may specifically be used for the detection of tertiary dentin. The influence of remaining dentin thickness, spatial arrangement of tissues, as well as

tissue properties on the visual projection of pulpal structures should be evaluated further in more *in vitro* as well as *in silico* studies.

With SWIRR, the cavity floor appeared homogenous and pulpal structures could not be differentiated during access preparation. The preparation floor appeared dark compared with the tooth's occlusal surface, indicating low backward reflection of photons. Nevertheless, with different wavelength tailored to the dentin-pulp complex or different preparation depth, there might be a possibility to visualize pulpal structures. Only open areas of the pulp chamber on the preparation floor were visible because the area appeared darker compared with the rest of the preparation cavity.

All of our results highlight that several landmarks can potentially be used for endodontic access navigation. To date, all endodontic navigation tools rely on cone-beam computed tomography or magnetic resonance imaging (Leontiev et al. 2021) to localize the pulp, either using a preoperatively constructed drill guide in case of static guidance or using optical tracking for drill orientation in the case of dynamic navigation (Connert et al. 2022). Both methods increase accuracy and reduce procedure time compared with freehand preparations (Connert et al. 2019; Zubizarreta-Macho et al. 2020); however, they present challenges such as obstructed visibility of the operation field and necessitate an elaborate preoperative workflow. SWIRT, on the other hand, could be seen as a new way of visual endodontic navigation by directly visualizing pulpal structures during access preparation. It can be performed live without any health concerns due to the absence of x-rays and does not require extensive preparation, thus eliminating the limiting factors of conventional navigation methods. However, it needs to be noted that camera systems are required due to the use of infrared light. Integrated into a surgical microscope (Simon et al. 2021), a comprehensive navigational system could be developed to combine magnification with navigation to first increase visibility in dentin, shown here, and later contrasts on the pulp chamber floor (Simon et al. 2021). The potential of such a system to improve accuracy and procedure time should be clinically evaluated in the future, together with dentists' ability to discriminate between pulpal and parapulpal areas.

By performing hierarchical cluster analysis on each segment, specific image features could be detected and clustered unsupervised. In such a navigational system, these patterns could be used for automatic area recognition and classification by either visualization or machine learning (Lambin et al. 2017; Avanzo et al. 2020) to determine the location of the pulp chamber and parapulpal areas. In this context, image biomarkers have already been successfully applied to CT and magnetic resonance imaging data in cancer research to increase diagnostic accuracy (Shin et al. 2022). Expanding the image features could improve these further.

Lastly, several study limitations need to be addressed. While our *ex vivo* model simulated a clinically relevant situation, only a relatively small number of samples was available. In addition, multiple analyses were performed on these

samples to validate their optical representations. On the other hand, they included a wide variety of characteristics such as a different overall anatomy, obliterations, and caries and include different restorations enhancing the generalizability of the results. Nevertheless, our observations were still consistent and objectifiable. *In vitro* and *in silico* analysis should be conducted in the future to delineate the full mechanism of the observed visual representation.

In summary, our results lay the groundwork for exploring the mechanism behind the visual representations and clinical application of SWIR technology as a noninvasive and radiation-free advanced imaging technique for endodontic access navigation. Nevertheless, further studies are needed to validate its efficacy in clinical settings to integrate this technique into the clinical routine.

Author Contributions

L. Benz, contributed to data investigation and interpretation, drafted the manuscript; K. Heck, contributed to methodology, data interpretation, critically revised the manuscript; D. Hevisov, contributed to data investigation and analysis, drafted the manuscript; D. Kugelmann, F. Litzemberger, J. Waschke, contributed to methodology, critically revised the manuscript; P.-C. Tseng, contributed to data investigation, drafted the manuscript; Z. Srejj, contributed to data investigation, critically revised the manuscript; F. Schwendicke, A. Kienle, R. Hickel, K.-H. Kunzelmann, contributed to data interpretation, critically revised the manuscript; E. Walter, contributed to conception, methodology, design, data investigation, analysis, and interpretation, drafted the manuscript. All authors have their final approval and agree to be accountable for all aspects of work.

Acknowledgment

We are grateful to Axel Unverzagt for his assistance with the body donors received by the Institute of Anatomy and Cell Biology, Ludwig-Maximilian-Universität München, Germany.

Declaration of Conflicting Interests


The authors declared no potential conflicts of interest with respect to the research, authorship, and/or publication of this article.

Funding

The authors disclosed receipt of the following financial support for the research, authorship, and/or publication of this article: The study was partly funded by the DFG (Deutsche Forschungsgemeinschaft) with grant number 494559609 to K.H. and F.L.

ORCID iDs

K. Heck  <https://orcid.org/0000-0003-2273-3662>

P.-C. Tseng  <https://orcid.org/0000-0002-1592-0905>

F. Litzemberger  <https://orcid.org/0009-0000-9423-8383>

F. Schwendicke  <https://orcid.org/0000-0003-1223-1669>

E. Walter  <https://orcid.org/0000-0003-4802-2279>

Data Availability

Original data are available after registration in our institutional open data repository <https://data.ub.uni-muenchen.de/477> with the DOI 10.5282/ubm/data.477 and the citation “Benz, Leander and Heck, Katrin and Walter, Elias: Data: Visualization of Pulpal Structures by SWIR in Endodontic Access Preparation. 29.04.2024. Open Data LMU. 10.5282/ubm/data.477.”

References

- Avanzo M, Wei L, Stancanello J, Vallières M, Rao A, Morin O, Mattonen SA, El Naqa I. 2020. Machine and deep learning methods for radiomics. *Med Phys.* 47(5):e185–e202.
- Berghammer K, Litzemberger F, Heck K, Kunzelmann KH. 2022. Attenuation of near-ultraviolet, visible and near-infrared light in sound and carious human enamel and dentin. *Clin Oral Investig.* 26(9):5847–5855. doi:10.1007/s00784-022-04541-7
- Carvalho TS, Lussi A. 2017. Age-related morphological, histological and functional changes in teeth. *J Oral Rehabil.* 44(4):291–298. doi:10.1111/joor.12474
- Connert T, Krug R, Eggmann F, Emsermann I, ElAyouti A, Weiger R, Kühl S, Krastl G. 2019. Guided endodontics versus conventional access cavity preparation: a comparative study on substance loss using 3-dimensional-printed teeth. *J Endod.* 45(3):327–331. doi:10.1016/j.joen.2018.11.006
- Connert T, Weiger R, Krastl G. 2022. Present status and future directions: guided endodontics. *Int Endod J.* 55(S4):995–1002. doi:10.1111/iej.13687
- Eleftheriadis GI, Lambrianidis TP. 2005. Technical quality of root canal treatment and detection of iatrogenic errors in an undergraduate dental clinic. *Int Endod J.* 38(10):725–734. doi:10.1111/j.1365-2591.2005.01008.x
- Fleig S, Attin T, Jungbluth H. 2017. Narrowing of the radicular pulp space in coronally restored teeth. *Clin Oral Investig.* 21(4):1251–1257. doi:10.1007/s00784-016-1899-8
- Fried D, Glens RE, Featherstone JDB, Seka W. 1995. Nature of light scattering in dental enamel and dentin at visible and near-infrared wavelengths. *Appl Opt.* 34(7):1278. doi:10.1364/AO.34.001278
- Heck K, Kunzelmann KH, Walter E, Kaisarly D, Hoffmann L, Litzemberger F. 2023. Proximal caries detection using short-wave infrared transillumination at wavelengths of 1050, 1200 and 1300 nm in permanent posterior human teeth. *Diagnostics.* 13(20):3257. doi:10.3390/diagnostics13203257
- Hong G, Antaris AL, Dai H. 2017. Near-infrared fluorophores for biomedical imaging. *Nat Biomed Eng.* 1:0010. doi:10.1038/s41551-016-0010
- Jud C, Schaff F, Zanette I, Wolf J, Fehringer A, Pfeiffer F. 2016. Dental tubules revealed with x-ray tensor tomography. *Dental Mater.* 32(9):1189–1195. doi:10.1016/j.dental.2016.06.021
- Kiefner P, Connert T, ElAyouti A, Weiger R. 2017. Treatment of calcified root canals in elderly people: a clinical study about the accessibility, the time needed and the outcome with a three-year follow-up. *Gerodontology.* 34(2):164–170. doi:10.1111/ger.12238
- Kienle A, Forster FK, Diebold R, Hibst R. 2003. Light propagation in dentin: influence of microstructure on anisotropy. *Phys Med Biol.* 48(2):N7–N14. doi:10.1088/0031-9155/48/2/401
- Kienle A, Michels R, Hibst R. 2006. Magnification—a new look at a long-known optical property of dentin. *J Dent Res.* 85(10):955–959. doi:10.1177/154405910608501017
- Lambin P, Leijenaar RTH, Deist TM, Peerlings J, De Jong EEC, Van Timmeren J, Sanduleanu S, Larue RTHM, Even AJG, Jochems A, et al. 2017. Radiomics: the bridge between medical imaging and personalized medicine. *Nat Rev Clin Oncol.* 14(12):749–762. doi:10.1038/nrclinonc.2017.141
- Langeland K. 1987. Tissue response to dental caries. *Dental Traumatol.* 3(4):149–171. doi:10.1111/j.1600-9657.1987.tb00619.x
- Lederer A, Kunzelmann KH, Heck K, Hicel R, Litzemberger F. 2019. In-vitro validation of near-infrared reflection for proximal caries detection. *Eur J Oral Sci.* 127(6):515–522. doi:10.1111/eos.12663
- León-López M, Cabanillas-Balsera D, Martín-González J, Montero-Miralles P, Saúco-Márquez JJ, Segura-Egea JJ. 2022. Prevalence of root canal treatment worldwide: a systematic review and meta-analysis. *Int Endod J.* 55(11):1105–1127. doi:10.1111/iej.13822
- Leontiev W, Bieri O, Madörin P, Dagassan-Berndt D, Kühn S, Krastl G, Krug R, Weiger R, Connert T. 2021. Suitability of magnetic resonance imaging for guided endodontics: proof of principle. *J Endod.* 47(6):954–960. doi:10.1016/j.joen.2021.03.011
- Nudel I, Pokhrajav A, Hausman BS, Bitterman Y, Shpack N, May H, Sarig R. 2020. Age estimation of fragmented human dental remains by secondary dentin virtual analysis. *Int J Legal Med.* 134(5):1853–1860. doi:10.1007/s00414-020-02366-1
- Patel S, Rhodes J. 2007. A practical guide to endodontic access cavity preparation in molar teeth. *Br Dent J.* 203(3):133–140. doi:10.1038/bdj.2007.682
- Shin J, Seo N, Baek SE, Son NH, Lim JS, Kim NK, Koom WS, Kim S. 2022. MRI radiomics model predicts pathologic complete response of rectal cancer following chemoradiotherapy. *Radiology.* 303(2):351–358. doi:10.1148/RADIOLOGY.211986
- Simon J, Mogire EO, Yun SY, Fried D. 2021. Multispectral SWIR images of the pulp-chamber of posterior teeth in vitro. *SPIE-Intl Soc Optical Eng.* 2021:11627:116270L. doi:10.1117/12.2584900
- Smith AJ, Cassidy N, Perry H, Bègue-Kim C, Ruch JV, Lesot H. 1995. Reactionary dentinogenesis. *Int J Dev Biol.* 39(1):273–280.
- Thimsen E, Sadtler B, Berezin MY. 2017. Shortwave-infrared (SWIR) emitters for biological imaging: a review of challenges and opportunities. *Nanophotonics.* 6(5):1043–1054. doi:10.1515/nanoph-2017-0039
- Tjäderhane L, Carrilho MR, Breschi L, Tay FR, Pashley DH. 2009. Dentin basic structure and composition—an overview. *Endod Topics.* 20(1):3–29. doi:10.1111/j.1601-1546.2012.00269.x
- Tsesis I, Rosenberg E, Faivishevsky V, Kfir A, Katz M, Rosen E. 2010. Prevalence and associated periodontal status of teeth with root perforation: a retrospective study of 2,002 patients’ medical records. *J Endod.* 36(5):797–800. doi:10.1016/j.joen.2010.02.012
- van Griethuysen JJM, Fedorov A, Parmar C, Hosny A, Aucoin N, Narayan V, Beets-Tan RGH, Fillion-Robin J-C, Pieper S, Aerts HJWL. 2017. Computational radiomics system to decode the radiographic phenotype. *Cancer Res.* 77(21):e104–e107. doi:10.1158/0008-5472.CAN-17-0339
- Yamaguchi M, Noiri Y, Itoh Y, Komichi S, Yagi K, Uemura R, Naruse H, Matsui S, Kuriki N, Hayashi M, et al. 2018. Factors that cause endodontic failures in general practices in Japan. *BMC Oral Health.* 18(1):70. doi:10.1186/s12903-018-0530-6
- Zoller CJ, Hohmann A, Foschum F, Geiger S, Geiger M, Ertl TP, Kienle A. 2018. Parallelized Monte Carlo software to efficiently simulate the light propagation in arbitrarily shaped objects and aligned scattering media. *J Biomed Opt.* 23(6):1–12. doi:10.1117/1.jbo.23.6.065004
- Zubizarreta-Macho Á, de Pedro Muñoz A, Riad Deglow E, Agustín-Panadero R, Mena Álvarez J. 2020. Accuracy of computer-aided dynamic navigation compared to computer-aided static procedure for endodontic access cavities: an in vitro study. *J Clin Med.* 9(1):129. doi:10.3390/jcm9010129